Noninvasive Quantification of Myocardial ^{11}C-*Meta*-Hydroxyephedrine Kinetics

Hendrik J. Harms[1], Marc C. Huisman[1], Mischa T. Rijnierse[2], Henri Greuter[1], Yu-Lung Hsieh[3], Stefan de Haan[2], Robert C. Schuit[1], Paul Knaapen[2], Mark Lubberink[1,4], and Adriaan A. Lammertsma[1]

[1]Department of Radiology and Nuclear Medicine, VU University Medical Center, Amsterdam, The Netherlands; [2]Department of Cardiology, VU University Medical Center, Amsterdam, The Netherlands; [3]Philips Healthcare, Cleveland, Ohio; and [4]Nuclear Medicine and PET, Uppsala University, Akademiska sjukhuset, Uppsala, Sweden

^{11}C-*meta*-hydroxyephedrine (^{11}C-HED) kinetics in the myocardium can be quantified using a single-tissue-compartment model together with a metabolite-corrected arterial blood sampler input function (BSIF). The need for arterial blood sampling, however, limits clinical applicability. The purpose of this study was to investigate the feasibility of replacing arterial sampling with imaging-derived input function (IDIF) and venous blood samples. **Methods:** Twenty patients underwent 60-min dynamic ^{11}C-HED PET/CT scans with online arterial blood sampling. Thirteen of these patients also underwent venous blood sampling. Data were reconstructed using both 3-dimensional row-action maximum-likelihood algorithm (3DR) and a time-of-flight (TF) list-mode reconstruction algorithm. For each reconstruction, IDIF results were compared with BSIF results. In addition, IDIF results obtained with venous blood samples and with a transformed venous-to-arterial metabolite correction were compared with results obtained with arterial metabolite corrections. **Results:** Correlations between IDIF- and BSIF-derived K_1 and V_T were high ($r^2 >$ =0.89 for 3DR and TF). Slopes of the linear fits were significantly different from 1 for K_1, for both 3DR (slope = 0.94) and TF (slope = 1.06). For V_T, the slope of the linear fit was different from 1 for TF (slope = 0.93) but not for 3DR (slope = 0.98). Use of venous blood data introduced a large bias in V_T (r^2 = 0.96, slope = 0.84) and a small bias in K_1 (r^2 = 0.99, slope = 0.98). Use of a second-order polynomial venous-to-arterial transformation was robust and greatly reduced bias in V_T (r^2 = 0.97, slope = 0.99) with no effect on K_1. **Conclusion:** IDIF yielded precise results for both 3DR and TF. Venous blood samples can be used for absolute quantification of ^{11}C-HED studies, provided a venous-to-arterial transformation is applied. A venous-to-arterial transformation enables noninvasive, absolute quantification of ^{11}C-HED studies.

Key Words: sympathetic innervation; ^{11}C-HED; absolute quantification; image derived input function; blood samples

J Nucl Med 2016; 57:1376–1381
DOI: 10.2967/jnumed.115.167437

Recently, interest in sympathetic innervation imaging using PET (*1–4*) or SPECT (*5*) has increased based on its potential to predict life-threatening arrhythmias (*6,7*). Sympathetic nerve terminals are more vulnerable to ischemic damage than cardiomyocytes, and consequently, in myocardial infarctions, the region of reduced sympathetic innervation often exceeds that of scar formation (mismatch) (*7–10*). In a preclinical study (*11*), this mismatch area was shown to be a predictor of inducible ventricular tachycardias, originating from these mismatch areas. Therefore, noninvasive imaging of sympathetic innervation may play a major role in risk stratification and treatment planning for patients with (ischemic) heart failure.

Sympathetic innervation can be measured using ^{11}C-*meta*-hydroxyephedrine (^{11}C-HED) (*1,2*), which has recently been used in prediction risk assessment of sudden cardiac arrest in patients with ischemic cardiomyopathy (*12*). ^{11}C-HED kinetics can be quantified (*13,14*), with the single-tissue-compartment model being the most robust method (*15*), potentially yielding more accurate and clinically more relevant information than qualitative analysis. To date, however, quantitative ^{11}C-HED studies require arterial blood sampling for measuring the metabolite-corrected arterial plasma input function. This, in turn, requires arterial cannulation, which is a burden to the patient and technically demanding; therefore, alternatives should be explored.

An alternative for arterial sampling is the use of an image-derived input function (IDIF), because large blood-pool structures (e.g., ascending aorta [AA], left ventricle) are in the field of view of the scanner. IDIFs have been used successfully for other tracers such as ^{15}O-H_2O and ^{18}F-FDG (*16,17*). In the case of ^{11}C-HED, a complexity is the rapid clearance from the blood in combination with high specific uptake in myocardial tissue, which essentially makes the large blood-pool structures cold spots within the scan at late time points. For this reason, spill-over and small inaccuracies in the reconstruction algorithm (e.g., scatter correction) can have large consequences for IDIF, and results obtained with other tracers cannot directly be extrapolated to ^{11}C-HED.

In addition, because ^{11}C-HED has significant metabolism within the study duration (*15*), input functions need to be corrected for the presence of radiolabeled metabolites. Large intersubject differences in ^{11}C-HED metabolism have been observed, and consequently, individual metabolite corrections are required. In theory, these corrections can be derived from venous samples, but evidence is emerging that there may be discrepancies between corrections obtained using arterial and venous blood for at least some tracers

Received Sep. 25, 2015; revision accepted Mar. 1, 2016.
For correspondence or reprints contact: Marc C. Huisman, Department of Radiology and Nuclear Medicine, VU University Medical Center, P.O. Box 7057, 1007 MB Amsterdam, The Netherlands.
E-mail: m.huisman@vumc.nl
Published online May 26, 2016.

(*18*). Therefore, the aim of this study was to assess whether ^{11}C-HED kinetics can be quantified reliably without arterial cannulation, using an IDIF and venous blood samples.

MATERIALS AND METHODS

Patient Population

Twenty patients (mean age, 69 y; age range, 50–82 y; 15 men) with ischemic or dilated cardiomyopathy and a left ventricular ejection fraction below 35%, as determined by cardiac MRI, were included in the study. Ischemic cardiomyopathy was defined as the presence of one or more stenoses greater than 50% on coronary angiography and delayed contrast enhancement on cardiac MRI. The study was approved by the local Medical Ethics Review Committee, and all participants gave written informed consent before inclusion.

Scanning Protocol

^{11}C-HED was synthesized as described previously (*15*). Studies were performed on a Gemini TF-64 PET/CT scanner (Philips Healthcare). A 60-min dynamic emission scan was started simultaneously with the injection of 370 MBq of ^{11}C-HED, administered as a 5-mL bolus (0.8 mL·s^{-1}) followed by a 35-mL saline flush (2 mL·s^{-1}). This emission scan was followed immediately by a respiration averaged low-dose CT scan during normal breathing.

Images were reconstructed into 36 frames, with all appropriate corrections applied, using either the standard 3-dimensional row-action maximum-likelihood algorithm (3DR) reconstruction protocol as implemented on the Gemini scanner or the latest version of the time-of-flight (TF) reconstruction protocol, which comes with Monte Carlo (*19*)–based scatter correction and will be implemented in the current generation of Philips scanners (Ingenuity TF) (*20*).

Input Functions

All patients received an indwelling radial artery catheter for arterial blood sampling during the dynamic emission scan. Using an online detection system (*21*), we continuously withdrew arterial blood at a rate of 5 mL·min^{-1} during the first 5 min and 1.7 mL·min^{-1} thereafter. In addition, 7-mL arterial blood samples were collected manually at 2.5, 5, 10, 15, 20, 30, 40, and 60 min after injection for all patients. For 13 patients, a set of 7 additional 7-mL venous blood samples was collected from the infusion line, simultaneously with the arterial blood samples. To avoid contamination of the venous blood samples, the infusion line was flushed with heparin before the first and after the withdrawal of each venous blood sample. Activity concentrations in plasma and whole blood were determined for each sample. In addition, plasma was analyzed for radiolabeled metabolites of ^{11}C-HED by solid-phase extraction as described previously (*15*).

All blood sampler and manually drawn blood sample data were corrected for decay. Blood sampler data were corrected for delay and dispersion by fitting the early part of the sampler curve to the AA time–activity curve as described previously (supplemental material [available at http://jnm.snmjournals.org]; (*15*)). Next, the resulting delay-corrected sampler curve was calibrated using the manually drawn arterial blood samples and corrected for plasma–to–whole-blood ratios and fractions of unmetabolized ^{11}C-HED (parent fraction) by fitting the data to sigmoid functions as described previously (*15*). An IDIF was obtained by multiplying the AA time–activity curve, obtained for each separate reconstruction, with the same sigmoid functions.

Venous blood samples were handled in the same way as arterial samples, and the resulting sigmoid functions were then applied to the AA time–activity curve to obtain an alternative IDIF. In addition, for both corrections, transformation factors from venous to arterial values were derived, using an empirically derived second-degree polynomial. These transformation factors were then applied to the raw data of the venous blood, and these transformed data were used similarly as described above to get a third IDIF, based on transformed venous blood data.

To correct for spill-over from the right ventricle (RV), a set of regions of interest (ROIs) was placed over the RV cavity in 5 consecutive transaxial planes, with ROI boundaries at least 1 cm away from the RV wall to avoid spill-over of myocardial activity. These ROIs were combined in a single RV volume of interest (VOI), which was then used to obtain the right ventricular time–activity curve ($C_{RV}(t)$). For all reconstructions, the same set of VOIs for both AA and RV VOIs was used.

Quantification of ^{11}C-HED Kinetics

Using software developed in-house with Matlab 7 (The Mathworks), we drew 16 myocardial segment VOIs on the final frame of the dynamic (3DR) scan, rotated to short-axis images, according to the 17-segment model of the American Heart Association, excluding the apex because this segment could not be delineated reliably in a large subset of the patients. Segmental time–activity curves were fitted to a single-tissue-compartment model using nonlinear least squares. Corrections for spill-over from left and RVs were included in the following model:

$$C_{PET}(t) = K_1 \times C_P(t) \otimes e^{-k_2 \times t} + V_A \times C_A(t) + V_{RV} \times C_{RV}(t) \quad \text{Eq. 1}$$

$C_{PET}(t)$, $C_A(t)$, and $C_{RV}(t)$ represent measured tissue, arterial blood, and right ventricular blood concentrations, respectively; $C_P(t)$ is the plasma activity concentrations of parent ^{11}C-HED; and K_1 and k_2 are the influx and clearance rate of ^{11}C-HED, respectively. V_A was assumed to be spill-over instead of arterial blood volume, because this implementation provides more accurate and robust parameter estimates (*15*). The total volume of distribution V_T was defined as K_1/k_2.

Segmental time–activity curves were fitted using nonlinear least squares and standard weighing factors. To exclude outliers or unreliable fits, only segments with parameter estimates with a coefficient of variation less than 25% were included. To eliminate differences in VOI definition, a single VOI template was used for all reconstructions.

Data Analysis

The area under the curve (AUC) was obtained for both whole BSIF and IDIF curves ($AUC_{0–60}$) and for early (0–1 min after injection [$AUC_{0–1}$]) and late (20–60 min after injection [$AUC_{20–60}$]) time intervals separately. AUCs were compared using paired *t* tests. Correlations between BSIF- and IDIF-derived K_1 and V_T and between arterial and venous data were assessed using linear regression with zero intercept, and a paired *t* test was used to test for significance of differences.

Transformation factors for venous data were validated by a direct comparison of K_1 and V_T values derived using arterial data and (transformed) venous data. In addition, to validate consistency of these transformation factors, patients were split in 2 subgroups, and for each group transformation factors were derived and applied to the data of the other subgroup. Because the effect of the metabolite correction is the same for 3DR and TF, the comparison between arterial and (transformed) venous data was performed only for 3DR.

RESULTS

Validation of IDIF

For 3 patients, online blood sampling failed because of technical reasons, and these patients were excluded for the comparison between BSIF and IDIF. Twenty-one segments were excluded because of a coefficient of variation greater than 25%, which after

visual inspection of both the time–activity curves and the dynamic images, appeared to be due to motion.

Population-averaged BSIF, 3DR IDIF ($IDIF_{3DR}$), and TF IDIF ($IDIF_{TF}$) data are presented in Figure 1, showing the first pass of the bolus through the left ventricle and late activity concentrations (Figs. 1A and 1B, respectively). $AUC_{0–60}$ was not significantly different for both $IDIF_{3DR}$ (367.2 kBq·mL^{-1}·min, $P = 0.258$) and $IDIF_{TF}$ (357.5 kBq·mL^{-1}·min, $P = 0.647$) when compared with BSIF $AUC_{0–60}$ (354.5 kBq·mL^{-1}·min). $AUC_{20–60}$ was not significantly different for $IDIF_{3DR}$, but it was increased for $IDIF_{TF}$ (73.9, 81.6, and 74.1 kBq·mL^{-1}·min for BSIF, $IDIF3_{DR}$, and $IDIF_{TF}$, respectively; $P = 0.007$ and 0.925 for $IDIF_{3DR}$ and $IDIF_{TF}$, respectively). Finally, $AUC_{0–1}$ was significantly different for $IDIF_{3DR}$ but not for $IDIF_{TF}$ (123.3, 127.0, and 136.3 kBq·mL^{-1}·min for BSIF, $IDIF3_{DR}$, and $IDIF_{TF}$, respectively; $P = 0.455$ and 0.001 for $IDIF_{3DR}$ and $IDIF_{TF}$, respectively). Figure 2 shows regression and Bland–Altman plots of K_1 obtained using BSIF and IDIF, for both 3DR and TF. For K_1, both reconstructions resulted in a similar correlation between IDIF- and BSIF-derived data ($r^2 = 0.91$, slope = 0.94 for 3DR; $r^2 = 0.91$, slope = 1.06 for TF). However, K_1 obtained using IDIF was different from that obtained using BSIF ($-4.9\% \pm 12.4\%$, $P < 0.001$ and $5.6\% \pm 11.2\%$, $P < 0.001$ for 3DR and TF, respectivley), and slopes of the linear fit were different from unity ($P < 0.001$ for both 3DR and TF).

Figure 3 shows similar plots for V_T. The correlation was significantly lower for 3DR than for TF ($r^2 = 0.89$ and 0.94 for 3DR and TF, respectively). The slope was not significantly different from unity for 3DR (slope = 0.98, $P = 0.13$), but it was for TF (slope = 0.93, $P < 0.001$). Similarly, differences between V_T obtained using BSIF and IDIF were significant for TF ($-6.0\% \pm 11.0\%$, $P < 0.001$) but not for 3DR ($-1.9\% \pm 14.9\%$, $P = 0.16$).

Validation of Venous Blood Samples

For 1 patient, venous samples could not be measured reliably because of technical reasons. For the remaining 12 patients, average arterial and venous plasma–to–whole-blood ratios and parent fractions are shown in Figure 4. It is clear that both plasma–to–whole-blood ratios and parent fractions differ significantly between arterial and venous data.

Figure 5 shows fits of plasma–to–whole-blood ratios and parent fractions for venous versus arterial data across all patients. There is a clear but nonlinear relationship between both datasets. Second-degree polynomials with free intercept for plasma–to–whole-blood ratio and intercept set to 0 for parent fraction were used to transform venous data. For the entire population, transformation equations were as follows:

$$PBR_{converted} = -0.68 \times PBR_{venous}{}^2 + 2.33 \times PBR_{venous} - 0.59 \quad \text{Eq. 2}$$

$$PF_{converted} = 0.35 \times PF_{venous}{}^2 + 0.62 \times PF_{venous} \quad \text{Eq. 3}$$

where PBR is plasma–to–whole-blood ratio, and PF is parent fraction.

Figure 6 shows correlation plots of K_1 and V_T for nontransformed and transformed venous data applied to $IDIF_{3DR}$. As can be seen, K_1 was estimated with high precision for both venous and transformed venous data ($r^2 = 0.99$ and 0.99) but with a small but significant bias ($-1.8\% \pm 2.1\%$ and $-2.3\% \pm 2.2\%$ for venous and transformed data, respectively, $P < 0.001$) and significant differences with K_1 obtained using arterial blood data ($P < 0.001$ for both). In contrast, V_T was estimated with a large bias when venous data were used ($r^2 = 0.96$, slope = 0.84, $P < 0.001$), which was reduced greatly when using transformed data ($r^2 = 0.97$, slope = 0.99, $P = 0.03$), and the paired t test showed no significant differences in V_T when transformed data were used (mean difference of $-12.6\% \pm 6.0\%$, $P < 0.001$ and $0.2\% \pm 6.4\%$, $P = 0.37$ for

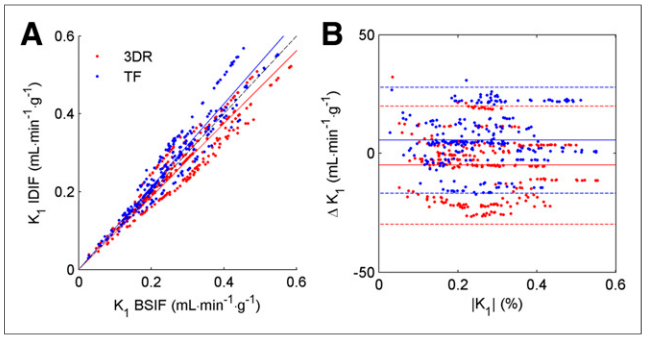

FIGURE 2. Correlation (A) and Bland–Altman (B) plots for K_1 obtained using BSIF and both $IDIF_{3DR}$ (red) and $IDIF_{TF}$ (blue). (A) Solid lines represent linear fits, and dashed lines indicate lines of identity. (B) Solid lines represent mean difference, and dashed lines indicate 95% confidence intervals.

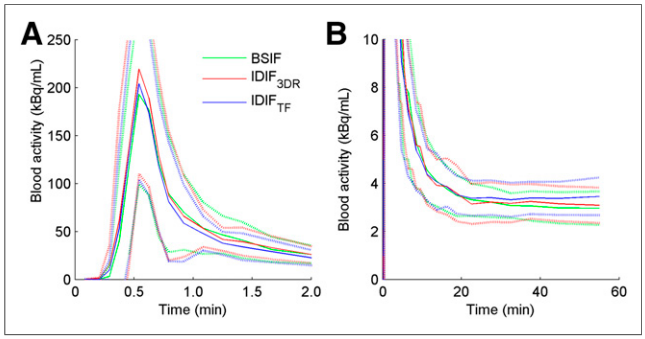

FIGURE 1. Population-averaged IDIF (red lines: 3DR; blue lines: TF) and BSIF (green lines) for peaks (A) and tails (B) of the curves. Dotted lines indicate mean ± SD.

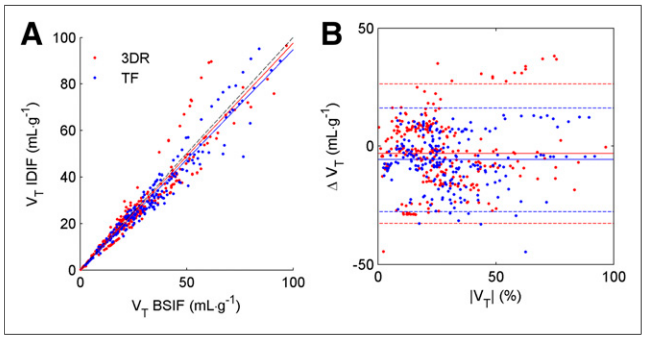

FIGURE 3. Correlation (A) and Bland–Altman (B) plots for V_T obtained using BSIF and both $IDIF_{3DR}$ (red) and $IDIF_{TF}$ (blue). (A) Solid lines represent linear fits, and dashed line is line of identity. (B) Solid lines represent mean difference, and dashed lines indicate 95% confidence intervals.

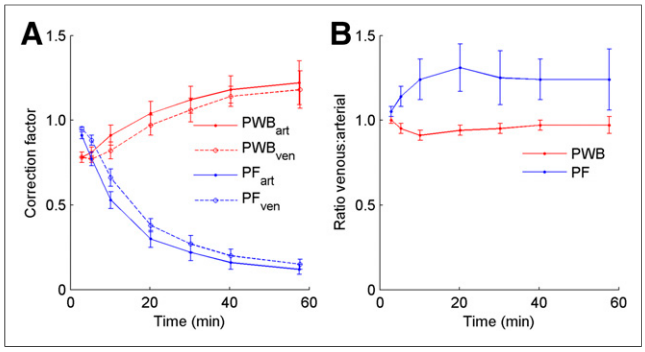

FIGURE 4. (A) Plasma–to–whole-blood ratio (PBR, red) and parent fraction (PF, blue) for arterial (PWB_{art} and PF_{art}, continuous lines) and venous (PWB_{ven} and PF_{ven}, dashed lines) blood samples as function of time. (B) Ratio of venous and arterial PBRs (red) and PFs (blue) as function of time.

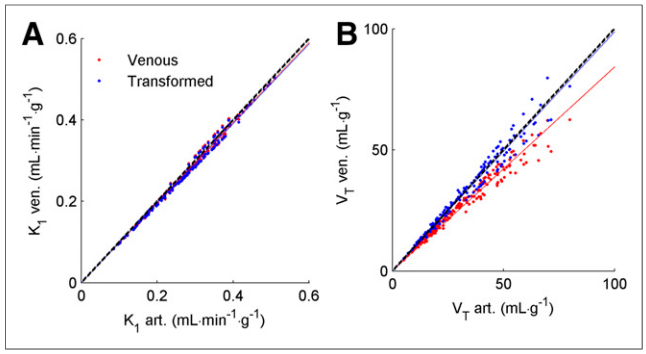

FIGURE 6. Correlation plots of K_1 (A) and V_T (B), calculated using venous (red) and transformed venous (blue) data, with corresponding parameters obtained using arterial data. Solid lines represent linear fits, and black dashed lines depict lines of identity.

venous and transformed data). For both transformed and nontransformed data, bias was consistent as indicated by the high correlations observed.

No significant differences were found when patients were split into 2 subgroups. When the transformation factors of subgroup 1 were applied to the data of subgroup 2 and vice versa, for both K_1 and V_T similar results were obtained as for the transformation factors based on data of all patients ($r^2 = 0.99$, slope = 1.02 for group 1 and $r^2 = 1.00$, slope = 0.96 for group 2 for K_1; $r^2 = 0.98$, slope = 0.98 for group 1 and $r^2 = 0.95$, slope = 0.98 for group 2 for V_T).

DISCUSSION

In the present study, an alternative to invasive (online) arterial blood sampling for quantification of ^{11}C-HED kinetics—that is, the use of an IDIF in combination with venous blood samples—was assessed. Using this method, ^{11}C-HED can be quantified without the need for additional arterial cannulation or, when using the infusion line for withdrawing the venous blood samples, any additional venous lines. The use of absolute quantification of ^{11}C-HED kinetics corrects for any biases due to metabolism or blood flow as might be present when using simplified measures such as retention index (*5*), although the need for arterial blood samples and online blood sampling has limited the use of fully quantitative ^{11}C-HED imaging. Clearly, less invasive methods of quantifying ^{11}C-HED kinetics are desired. A population-based metabolite correction introduced biases of up to 40% in individual patients (*15*), ruling out its use for ^{11}C-HED. This study, however, shows that use of venous blood samples and IDIF was accurate in quantifying ^{11}C-HED kinetics, reducing the invasiveness to solely having to apply a venous line for tracer infusion and withdrawal of venous blood samples.

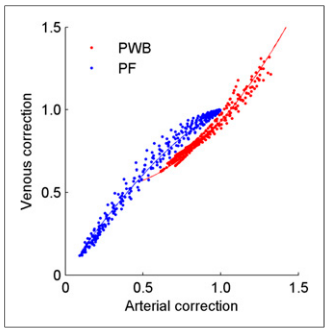

FIGURE 5. Correlation factors for plasma–to–whole-blood ratio (PWR, red dots) and parent fraction (PF, blue dots) derived from arterial (horizontal axis) and venous (vertical axis) blood data. Lines indicate fits derived using a second-order polynomial, of which inverse was used to transform venous data into arterial data (Eqs. 2 and 3).

$IDIF_{3DR}$ resulted in no bias for V_T and a small, but consistent, bias for K_1 when results were compared with those obtained using a BSIF. For $IDIF_{TF}$, a small but consistent bias was found for both K_1 and V_T. In addition, when venous blood samples were used to correct for both plasma-to-blood ratios and radiolabeled metabolites, a large but consistent bias was seen in V_T, but not in K_1. This bias in V_T was no longer significant when transformation factors were applied to venous blood data, and K_1 could still be calculated with no bias when transformation factors were applied.

Bias in K_1 when using an IDIF is expected based on the slight but significant overestimation of blood activity in the early phase (AUC_{0-1}) for IDIF when compared with BSIF, which is assumed to be a gold standard. At present, the reasons for the observed difference in early blood activities between $IDIF_{3DR}$ and BSIF remain unclear. Small errors in delay or dispersion correction of BSIF are not expected to introduce a difference in total activity (i.e., AUC). In addition, the injected dose was chosen to remain well within the linear range of the scanner in which dead-time corrections are still reliable, up to about 35 Mcps. Although scatter corrections were shown to yield accurate estimates of activity in a cold spot within a region with high activity, residual inaccuracies in absolute scaling of scatter corrections during the first pass, in which all activity is present in a small volume, cannot be excluded. Similar discrepancies were found in other studies that performed absolute quantification of ^{11}C-HED kinetics (*13,14*). These studies used a combination of blood sampler and image-derived data, using the left atrium, because IDIF suffered from increased spill-over during late time points and BSIF suffered from a significant apparent loss during early time points (*14*). This is similar to the results of the present study for early activity, showing a discrepancy in early activity between BSIF and IDIF although it is unclear whether this is an apparent loss in BSIF or an overestimation in IDIF. As in the present study, the AA rather than the left atrium was used for definition of IDIF, spill-over was not an issue, which is in line with results obtained with ^{18}F-FDG (*17*). Use of the AA should eliminate the main reason mentioned by Schafers et al. (*14*) for using an online blood sampling system. These studies, however, did not directly compare V_T and K_1 values derived using IDIF and BSIF data, as was performed in our study.

In this study, arterial activity was assumed to be spill-over from the arterial blood pool, rather than activity originating from an arterial blood volume fraction in the myocardium (*15*). In addition, a bias in IDIF results was observed (data not shown) when arterial activity was considered blood volume.

K_1 was significantly correlated to both the simplified innervation marker RI ($r^2 = 0.83$, $P < 0.001$) and the V_T ($r^2 = 0.44$, $P < 0.001$). Considering that K_1 itself can be used as a marker of myocardial blood flow in this patient group (*22*), this suggests that both innervation parameters have a significant contribution of myocardial blood flow to their signal and this has to be considered. However, the strength of the correlation was significantly higher for retention index than for V_T, advocating use of V_T as a less flow-dependent marker of innervation.

In addition to an accurate measurement of arterial blood concentrations, blood sample data are required for corrections for the presence of radiolabeled metabolites, yielding the final plasma input function. The gold standard approach to obtain such corrections is to use data from arterial blood samples. In the present study, using data from venous blood samples had no significant effect on derived K_1 values, as indicated by the excellent correlation and slope of the linear fit between K_1 values derived from arterial and venous blood samples. In contrast, it introduced a large bias in V_T values, as indicated by a slope of the linear fit of 0.84. This is not unexpected because K_1 is estimated from the early phase of the scan, during which metabolism has no significant effect and plasma-to-blood ratios are similar in arterial and venous blood (Fig. 4B). In contrast, V_T is estimated from the late phase of the scan in which the effects of metabolism are significant and differences in arterial and venous data are more pronounced (Fig. 4B). Given that in most cases V_T will be the most important ^{11}C-HED parameter, data from venous samples cannot be used directly to estimate V_T. Therefore, an attempt was made to transform venous data into data representing arterial data using an empiric transformation to fit both venous plasma–to–whole-blood ratio and parent fraction data to corresponding arterial data (Fig. 5). This transformation resulted in small to no biases in V_T or K_1 (slope of the linear fit of 0.99, $P = 0.03$ for V_T; slope of 0.98, $P < 0.001$ for K_1). To illustrate consistency of these transformation factors, patients were randomly split into 2 subgroups, and transformation factors were derived for each subgroup and then applied to the other subgroup. No significant differences in correlation or slopes of the linear fits were found between both subgroups and the entire patient population (data not shown), suggesting that these transformation factors are not specific for the individual patient.

There are some limitations in this study that need to be acknowledged. First, the number of patients included was small, and acquisition of both arterial and venous samples was not performed in all patients. In addition, whereas the transformation factors derived for the venous blood samples were accurate in this patient group, other patient groups might show different levels of metabolism, which potentially affects these factors in those groups. Similarly, the need for venous blood samples might limit applicability of quantitative ^{11}C-HED studies to institutes with blood analysis capabilities. However, because of the significant intersubject variation in ^{11}C-HED metabolism as described previously (*15*), omitting all metabolite corrections or using population-averaged data is not recommended because it may lead to severe biases in at least some patients. Venous blood samples correct for this and can be withdrawn from the tracer infusion line, making the method as noninvasive as simplified measures such as RI (*4*).

Finally, because the model implementation used in this study corrects only for spill-over of blood activity (*15*), some partial-volume effects remain. The magnitude of these effects are in theory dependent on, for instance, image resolution, regional wall-thickness and motion, and ROI size. As shown before, it is unprecise to use the same factor V_A for both spill-over and blood volume. Alternative correction factors, such as the perfusable or anatomic tissue fraction derived from a separate ^{15}O-water or ^{15}O-CO scan (*23*), can be explored to obtain more accurate estimates of innervation.

CONCLUSION

$IDIF_{3DR}$ and $IDIF_{TF}$ yielded precise results albeit with a small bias. In addition, venous blood samples can be used for absolute quantification of ^{11}C-HED kinetics, provided that a venous-to-arterial transformation is applied. This suggests that for patients with ischemic or dilated cardiomyopathy, absolute quantification of ^{11}C-HED kinetics can be performed noninvasively, enabling a more comprehensive analysis of sympathetic innervation without arterial cannulation.

DISCLOSURE

The costs of publication of this article were defrayed in part by the payment of page charges. Therefore, and solely to indicate this fact, this article is hereby marked "advertisement" in accordance with 18 USC section 1734. This work was supported financially by Philips Healthcare. No other potential conflict of interest relevant to this article was reported.

ACKNOWLEDGMENTS

We thank Amina Elouahmani, Femke Jongsma, Judith van Es, Nazerah Sais, Nghi Pham, Robin Hemminga, and Suzette van Balen for scanning patients; Kevin Takkenkamp and Marissa Rongen for analyzing blood; and Martien Mooijer, Jonas Eriksson, Anneloes Rijnders, Rolf van Kooij, and Johan van den Hoek for synthesizing ^{11}C-HED.

REFERENCES

1. Goldstein DS, Chang PC, Eisenhofer G, et al. Positron emission tomographic imaging of cardiac sympathetic innervation and function. *Circulation.* 1990; 81:1606–1621.
2. Münch G, Nguyen NT, Nekolla S, et al. Evaluation of sympathetic nerve terminals with [^{11}C]epinephrine and [^{11}C]hydroxyephedrine and positron emission tomography. *Circulation.* 2000;101:516–523.
3. Rosenspire KC, Haka MS, Van Dort ME, et al. Synthesis and preliminary evaluation of carbon-11-meta-hydroxyephedrine: a false transmitter agent for heart neuronal imaging. *J Nucl Med.* 1990;31:1328–1334.
4. Schwaiger M, Kalff V, Rosenspire K, et al. Noninvasive evaluation of sympathetic nervous system in human heart by positron emission tomography. *Circulation.* 1990;82:457–464.
5. Kline RC, Swanson DP, Wieland DM, et al. Myocardial imaging in man with I-123 meta-iodobenzylguanidine. *J Nucl Med.* 1981;22:129–132.
6. Paul M, Schafers M, Kies P, et al. Impact of sympathetic innervation on recurrent life-threatening arrhythmias in the follow-up of patients with idiopathic ventricular fibrillation. *Eur J Nucl Med Mol Imaging.* 2006;33:866–870.
7. Yukinaka M, Nomura M, Ito S, Nakaya Y. Mismatch between myocardial accumulation of ^{123}I-MIBG and ^{99m}Tc-MIBI and late ventricular potentials in patients after myocardial infarction: association with the development of ventricular arrhythmias. *Am Heart J.* 1998;136:859–867.
8. Inoue H, Zipes DP. Results of sympathetic denervation in the canine heart: supersensitivity that may be arrhythmogenic. *Circulation.* 1987;75:877–887.
9. Jacobson AF, Senior R, Cerqueira MD, et al. Myocardial iodine-123 meta-iodobenzylguanidine imaging and cardiac events in heart failure: results

of the prospective ADMIRE-HF (AdreView Myocardial Imaging for Risk Evaluation in Heart Failure) study. *J Am Coll Cardiol.* 2010;55:2212–2221.
10. Kammerling JJ, Green FJ, Watanabe AM, et al. Denervation supersensitivity of refractoriness in noninfarcted areas apical to transmural myocardial infarction. *Circulation.* 1987;76:383–393.
11. Sasano T, Abraham MR, Chang KC, et al. Abnormal sympathetic innervation of viable myocardium and the substrate of ventricular tachycardia after myocardial infarction. *J Am Coll Cardiol.* 2008;51:2266–2275.
12. Fallavollita JA, Heavey BM, Luisi AJ Jr, et al. Regional myocardial sympathetic denervation predicts the risk of sudden cardiac arrest in ischemic cardiomyopathy. *J Am Coll Cardiol.* 2014;63:141–149.
13. Rimoldi OE, Drake-Holland AJ, Noble MI, Camici PG. Basal and hyperaemic myocardial blood flow in regionally denervated canine hearts: an in vivo study with positron emission tomography. *Eur J Nucl Med Mol Imaging.* 2007;34:197–205.
14. Schäfers M, Dutka D, Rhodes CG, et al. Myocardial presynaptic and postsynaptic autonomic dysfunction in hypertrophic cardiomyopathy. *Circ Res.* 1998;82:57–62.
15. Harms HJ, de Haan S, Knaapen P, et al. Quantification of [^{11}C]-meta-hydroxyephedrine uptake in human myocardium. *EJNMMI Res.* 2014;4:52.
16. Iida H, Rhodes CG, De Silva R, et al. Use of the left ventricular time-activity curve as a noninvasive input function in dynamic oxygen-15-water positron emission tomography. *J Nucl Med.* 1992;33:1669–1677.
17. van der Weerdt AP, Klein LJ, Boellaard R, Visser CA, Visser FC, Lammertsma AA. Image-derived input functions for determination of MRGlu in cardiac ^{18}F-FDG PET scans. *J Nucl Med.* 2001;42:1622–1629.
18. Greuter HN, Lubberink M, Hendrikse N, et al. Venous versus arterial blood samples for plasma input pharmacokinetic analysis of different radiotracer PET studies [abstract]. *J Nucl Med.* 2011;52(suppl 1):1974.
19. Reddin J, Scheuermann J, Perins A, Karp J. Quantitative evaluation of Monte Carlo scaling applied to single scatter simulation (SSS-MC) [abstract]. *J Nucl Med.* 2015;56(suppl 3):263.
20. Kolthammer JA, Su KH, Grover A, Narayanan M, Jordan DW, Muzic RF. Performance evaluation of the Ingenuity TF PET/CT scanner with a focus on high count-rate conditions. *Phys Med Biol.* 2014;59:3843–3859.
21. Boellaard R. van LA, van Balen SC, Hoving BG, Lammertsma AA. Characteristics of a new fully programmable blood sampling device for monitoring blood radioactivity during PET. *Eur J Nucl Med.* 2001;28:81–89.
22. Harms HJ, Lubberink M, de Haan S, et al. Use of a single [^{11}C]-*meta*-hydroxyephedrine scan protocol for assessing flow-innervation mismatches in patients with ischemic cardiomyopathy. *J Nucl Med.* 2015;56:1706–1711.
23. Harms HJ, de Haan S, Knaapen P, Allaart CP, Lammertsma AA, Lubberink M. Parametric images of myocardial viability using a single ^{15}O-H2O PET/CT scan. *J Nucl Med.* 2011;52:745–749.